

Water Resources Research®

RESEARCH ARTICLE

10.1029/2021WR031886

Key Points:

- Geometry of larger-scale facies types is most relevant to explain effective dispersion and mixing processes
- The effect of sediment properties and univariate statistics of K on mixing and effective dispersion and their uncertainty are evaluated
- Dispersion process is more realization dependent than mixing process

Supporting Information:

Supporting Information may be found in the online version of this article.

Correspondence to:

Z. Dai and M. R. Soltanian,
dzx@jlu.edu.cn;
soltanian@uc.edu

Citation:

Ren, W., Ershadnia, R., Wallace, C. D., LaBolle, E. M., Dai, Z., de Barros, F. P. J., & Soltanian, M. R. (2022). Evaluating the effects of multiscale heterogeneous sediments on solute mixing and effective dispersion. *Water Resources Research*, 58, e2021WR031886. <https://doi.org/10.1029/2021WR031886>

Received 29 DEC 2021

Accepted 5 SEP 2022

Author Contributions:

Conceptualization: Zhenxue Dai, Mohamad R. Soltanian

Data curation: Reza Ershadnia

Formal analysis: Wanli Ren, Reza Ershadnia

Funding acquisition: Zhenxue Dai

Methodology: Zhenxue Dai, Felipe P. J. de Barros, Mohamad R. Soltanian

Resources: Mohamad R. Soltanian

Software: Wanli Ren, Corey D. Wallace, Eric M. LaBolle





Supervision: Zhenxue Dai

Visualization: Wanli Ren, Reza Ershadnia, Corey D. Wallace

Writing – original draft: Wanli Ren, Reza Ershadnia

Writing – review & editing: Corey D. Wallace, Eric M. LaBolle, Zhenxue Dai, Felipe P. J. de Barros, Mohamad R. Soltanian

Evaluating the Effects of Multiscale Heterogeneous Sediments on Solute Mixing and Effective Dispersion

Wanli Ren^{1,2}, Reza Ershadnia² , Corey D. Wallace^{2,3}, Eric M. LaBolle⁴, Zhenxue Dai¹ , Felipe P. J. de Barros⁵ , and Mohamad R. Soltanian^{2,6} 

¹College of Construction Engineering, Jilin University, Changchun, Jilin, China, ²Department of Geology, University of Cincinnati, Cincinnati, OH, USA, ³Geosyntec Consultants, Columbus, OH, USA, ⁴Department of Hydrologic Sciences, University of California, Davis, CA, USA, ⁵Sonny Astani Department of Civil and Environmental Engineering, University of Southern California, Los Angeles, CA, USA, ⁶Department of Environmental Engineering, University of Cincinnati, Cincinnati, OH, USA

Abstract The heterogeneity of sedimentary aquifers can be characterized by parameters related to the underlying sedimentary structure such as physical attributes of sediments (e.g., volume proportions and lengths of facies types). These parameters often reflect multiscale variability typically observed in the hydraulic conductivity field and the resulting fluid velocity. Although there have been many studies of solute transport processes (e.g., dispersion, mixing, and dilution) in heterogeneous media, there is still a lack of understanding of the controlling influence of sedimentary architecture on the time-evolution of the solute plume's spreading and mixing behavior and their uncertainty. In this work, we used high-resolution and three-dimensional numerical simulations to investigate the time-evolution of the effective dispersion and mixing behavior of the solute through a heterogeneous aquifer that displays multiscale sedimentary architecture. Transport simulations are performed by using the random walk particle tracking method. Our numerical experiments allow us to understand which scale of sedimentary architecture is most relevant to explaining effective dispersion and mixing. We further analyze whether or not the uncertainty in solute spreading and mixing are equally affected by the different spatial organization of sedimentary facies types. We also perform an extensive parametric study to better understand the effect of physical sediment attributes and univariate statistics of hydraulic conductivity (e.g., mean and variance) at the facies scale on both effective dispersion and mixing. Our results indicate that meter-scale heterogeneity plays a major role in controlling solute transport processes. Moreover, the effective dispersion is more sensitive to the spatial organization of sedimentary facies type.

1. Introduction

Accurate representation of solute transport processes (e.g., dispersion, mixing, and dilution) is important for various porous media-related applications such as hydrogeology, soil physics, environmental engineering and sciences, water resources management, and petroleum engineering (de Barros et al., 2015; Ershadnia, Hajirezaie, et al., 2021; Ershadnia, Wallace, et al., 2021; Fiori & Dagan, 2000; Fiori, 2001; Jha et al., 2011; Jiménez-Martínez et al., 2015; Kitanidis and McCarty, 2012). Large-scale field experiments (e.g., Borden, MADE, Cape Cod) have revealed that spatial heterogeneity in physical and geochemical sediment properties, as well as local-scale dispersion, are among the primary underlying mechanisms which govern solute transport processes (Anderson & McCray, 2011; Attinger et al., 2004; Bianchi et al., 2011; Dai et al., 2004; Fiori & Dagan, 1999; Freyberg, 1986; Gelhar, 1986; Ritzi & Soltanian, 2015; Salamon et al., 2007; Sudicky & Illman, 2011; Zheng et al., 2011). Heterogeneous aquifer hydraulic conductivity (K) results in erratic solute distributions, which increase solute surface area and enhance spreading and mixing (Burr et al., 1994; de Barros et al., 2015; Dentz et al., 2011, 2018; Kitanidis, 1994; Sanchez-Vila et al., 2006; Werth et al., 2006). It is therefore important to understand which scales and aspects of sediment heterogeneity should be incorporated into groundwater flow and solute transport models to improve prediction performance while also reducing the uncertainty associated with data paucity.

In this article, we analyze dispersion, mixing, and dilution processes as they occur in groundwater flow within heterogeneous sedimentary deposits. Such deposits are often comprised of sedimentary facies types (i.e., three-dimensional, 3D, bodies of sediments as per Soltanian & Ritzi, 2014) defined at varying scales, resulting in a multiscale spatial organization (i.e., sedimentary architecture) (see Figure S1 in Supporting Information S1). Thus, spatial variability in K based on such heterogeneity models can create spatial structures that resemble

the multiscale architecture of sedimentary deposits (see Figure S2 in Supporting Information S1) (e.g., Dai et al., 2004, 2014, 2018; Soltanian, Ritzi, Dai, et al., 2015a; Soltanian, Ritzi, Huang, et al., 2015b).

Using indicator geostatistics, several works have provided a more realistic link between sedimentary architecture data (e.g., mean length and volume proportions of facies types) at different scales and the time-evolution of solute transport metrics (e.g., Dai et al., 2004; 2019, 2020; Ramanathan et al., 2010; Ritzi & Soltanian, 2015; Soltanian, Ritzi, Dai, et al., 2015a; Soltanian et al., 2020). The most important insight from these studies is that the spatial-bivariate correlation structure of K is directly defined by the transition probability structure (i.e., probability of transitioning from one facies type to another), with the main contributions from cross-transition probability. Moreover, the cross-distribution probabilities can be effectively modeled using quantifiable physical sediment properties (e.g., mean length, volume proportion). The geostatistical framework elaborated by the abovementioned works allows us to relate dispersion metrics and dilution to identifiable physical attributes of the underlying sedimentary architecture (e.g., Ramanathan et al., 2010; Soltanian et al., 2020).

A common approach to represent multiscale variability within groundwater flow and transport models is to use dispersion coefficients (e.g., Dagan, 1984; Dentz et al., 2000a, 2000b; Di Dato et al., 2016; Neuman et al., 1987; Rajaram & Gelhar, 1993; Rubin, 2003), which capture the effects of spatial velocity variability on transport processes. There are two commonly used dispersion coefficients in the literature: the ensemble and effective dispersions (see de Barros and Dentz, 2016 and references therein). Ensemble dispersion coefficient (D^{ens}) is calculated in terms of the second moment of the ensemble-averaged solute concentration field (Dagan, 1988; Gelhar & Axness, 1983; Rubin et al., 1999), whereas effective dispersion coefficient (D^{eff}) is computed in terms of the average over the centered second spatial moments of the solute plume in individual aquifer realizations (Attinger et al., 1999; Bellin et al., 1994; Dagan, 1990, 1991; Dentz et al., 2000a, 2000b; Kitanidis, 1988; Rajaram & Gelhar, 1993).

Dai et al. (2004) have developed a multiscale and anisotropic covariance model within Dagan's Lagrangian-based model (Dagan, 1989) to derive D^{ens} for transport of nonreactive solutes in multiscale deposits. Their model represents multifacies architecture within one scale of heterogeneity, which means their model is based on the statistical information of K and sediment properties on one scale to characterize the macroscopic dispersion. Ramanathan et al. (2010) extended the study by incorporating two scales of heterogeneity within the same model. They tested the performance of their model against observed tracer data from the natural gradient tracer test at the Borden site. Although their model used highly resolved sedimentary architecture data to represent the observed dispersion of the tracer data, their use of D^{ens} overestimated the observed data due to sample-to-sample fluctuation of the center of mass position of the solute plume. In addition, though these existing studies have significantly enhanced our understanding of the relationships between underlying sedimentary architecture and transport processes, they do not address the time-evolution and scale dependency of D^{eff} and solute mixing metrics (e.g., degree of mixing and dilution), particularly their associated uncertainty.

The benefits of using D^{eff} lie in its ability to better capture the dispersion process in nonergodic transport conditions, in which the characteristic solute plume initial dimensions are of the same order as the scale of heterogeneity. In such conditions, dispersion coefficients are prone to uncertainty. Expressions providing the functional relationship between the variance of the effective dispersion coefficient and the source dimensions in both 2D and 3D are provided in de Barros and Rubin (2011), Dentz and de Barros (2013), and de Barros and Dentz (2016). Those theoretical and numerical modeling studies of D^{eff} often characterize log- K ($Y = \ln(K)$) using unimodal formulations without considering the role of underlying sedimentary architecture and its multiscale nature. As Sanchez-Vila and Fernández-García (2016) pointed out, any model that hopes to resemble reality must incorporate as much detailed geology as possible.

This work is a logical extension of the aforementioned studies on both D^{eff} and D^{ens} . The goal is to provide a better understanding of the time-evolution and uncertainty of D^{eff} and solute mixing and dilution in multiscale sedimentary deposits. We investigate which scale of sedimentary architecture is most relevant to explaining solute transport processes. This article also addresses the following fundamental question: How does uncertainty in different numerically generated realizations of sedimentary architecture, and thus the corresponding K realizations, impact both D^{eff} and solute mixing? Further, is mixing equally affected by different spatial organization of sedimentary facies types as D^{eff} is? In addition, we perform an extensive parametric study to better understand the effect of physical sediment attributes and univariate facies statistics of K on both D^{eff} and mixing. We address these questions by developing multiscale and 3D numerical models using highly resolved and available sedimentary

Table 1

Hierarchy of Facies Types, and Univariate Statistics for Hydraulic Conductivity at Different Scales (Modified From Ramanathan et al., 2010)

Scale	Facies type	Description	p_o	\bar{l}_o	\bar{l}_z	\bar{Y}	σ_Y^2
Scale II	M	Associations of scale I facies MLD, MLF, and MM	0.39	3.0	0.18	2.06	0.25
	FZ	Associations of scale I facies FLD, FLF, FM, and Z	0.61	5.85	0.3	1.22	0.17
Scale I	MLD	Medium sand, distinct lamination	0.19	1.71	0.14	2.13	0.23
	MLF	Medium sand, faint lamination	0.09	0.9	0.06	1.90	0.30
	MM	Medium sand, massive	0.12	1.03	0.08	2.15	0.17
	FLD	Fine sand, distinct lamination	0.29	1.69	0.08	1.18	0.10
	FLF	Fine sand, faint lamination	0.23	1.88	0.08	1.30	0.16
	FM	Fine sand, massive	0.07	0.89	0.05	1.37	0.30
	Z	Silt	0.01	0.65	0.05	0.71	0.56

Note. Shown are proportions (p_o) of facies types, mean length in horizontal (\bar{l}_o) and vertical directions (\bar{l}_z), and mean (\bar{Y}) and variance (σ_Y^2) of natural log transform of K , $Y = \ln(K)$. Mean length, l , is in meters. Hydraulic conductivity is in m/day.

architecture data from the Borden aquifer (e.g., Ramanathan et al., 2010; Ritzi et al., 2013). We then compare the model results to the reported dispersion and dilution of nonreactive plumes from the tracer test conducted at the Borden site (Burr et al., 1994; Sudicky, 1986).

2. Method

2.1. Sedimentary Architecture and Geological Random Space Function Models

Geologic models are developed from observations at the Borden site (Ritzi et al., 2013), which include collocated samples of Y , volume proportions, and length statistics for sedimentary facies types at two mutually exclusive spatial scales (see Figures S1 and S2 in Supporting Information S1). The Borden site is the only site for which there is both high-quality tracer test data (Sudicky, 1986), and quantitative characterization of the sedimentary architecture (in both vertical and horizontal directions). There are two hierarchical levels of texturally defined sedimentary facies (scale I and II). The scales are numbered by increasing size. The larger-scale II facies (medium sand, denoted by M, and fine sand and silt, denoted by FZ) are comprised of the smaller-scale I facies (Table 1). Facies descriptions for both scales were quantified using approximately 9,800 geologic observations collected along a 30.5 m transect parallel (Ramanathan et al., 2010) to the axis of the well-documented Borden tracer tests (Mackay et al., 1986). The univariate statistics for Y at different scales were quantified by Ritzi et al. (2013).

Following the approach of Proce et al. (2004), geostatistical characterization, modeling, and simulation of the sedimentary architecture were performed in three stages using a transition probability geostatistical code (T-PROGS) (Carle, 1999). First, scale II (M and FZ facies types) volume proportions and length statistic data were used to develop Markov chain models in each of three principal directions. The Markov chain models were then used in transition probability indicator simulation with co-kriging and a quenching step to create a set of realizations of scale II facies architecture. In the second step, the scale I proportions and length statistics were used to create another set of realizations of smaller-scale strata similarly. Finally, scale I facies types were mapped into the corresponding scale II regions to create multiscale heterogeneity realizations. The final combined indicator realizations (called multiscale hereafter) and scale II indicator realizations (called scale II hereafter) (one realization of each scale is shown in Figure 1) were used to create K fields using univariate statistics (Table 1) reported by Ritzi et al. (2013) and were then used in flow and transport simulations, as described below. The simulation domain is 120 m long, 30 m wide, and 5 m thick, with a uniform cell size of 0.3, 0.3, and 0.02 m in the x -, y -, and z -directions, respectively. The global horizontal and vertical integral scale of Y are $\lambda_H = 2.11$ m and $\lambda_V = 0.12$ m, respectively (Ramanathan et al., 2010). Thus, the grid cell size is approximately $0.15 \lambda_Y$ in each direction. The resulting high-resolution grid (10 million grid cells) is necessary to capture small-scale strata at scale I. In all T-PROGS made realizations, the facies type with a higher proportion was represented as a background. The anisotropy ratio is 0.06 as quantified by facies length statistics in Table 1 (also see related discussion by Ramanathan et al., 2010).

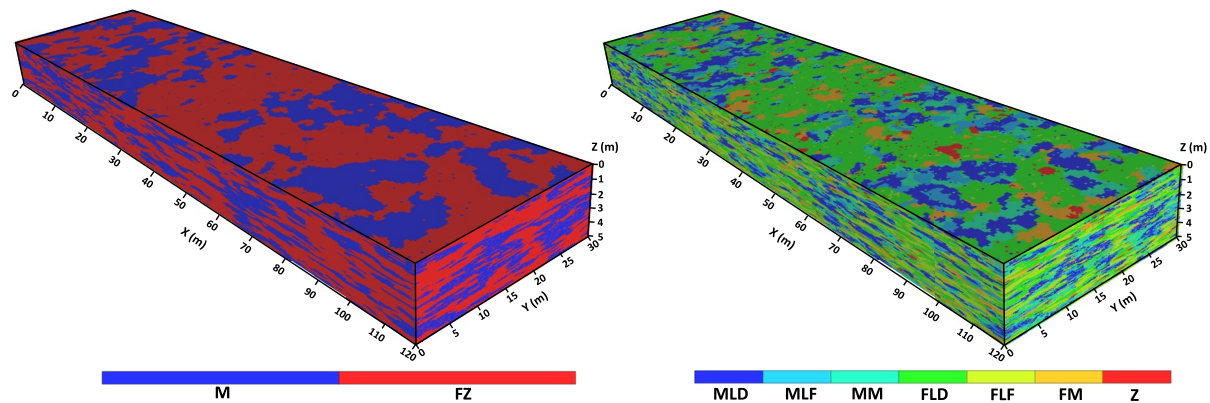


Figure 1. A realization of the sedimentary architecture was created using facies volume proportions and length statistics observed at the Borden site. The left panel shows a realization of larger-scale facies types of medium sand (M) and fine sand and silt (FZ) (scale II). The right panel shows multiscale representation and depicts smaller scale facies at scale I as they occur within the scale II facies types. Table 1 shows the description of scale I facies types.

We do not seek to perfectly match model results to the measured transport parameters given the potential sources of bias in the Borden tracer data and in the data used to develop the model parameters (see related discussion in Soltanian, Ritzi, Dai, et al., 2015a; Soltanian, Ritzi, Huang, et al., 2015b; Soltanian et al., 2020). Instead, we focus on general behaviors and uncertainties in the estimation of spreading and mixing metrics described below. We compare flow and transport simulations that include multiscale and only scale II representations of the sedimentary architecture to understand which numerically generated scale control dispersion and mixing. Furthermore, we investigate the influence of heterogeneous structure parameters as well as univariate statistics of Y on solute transport and associated uncertainties based on scale II realizations to understand the most important aspect of heterogeneity.

2.2. Flow and Mass Transport Simulators

The 3D finite-difference groundwater flow simulations were conducted using MODFLOW-2005 (Harbaugh, 2005) to calculate the velocity field of steady-state flow. The aquifer domain shared the same grid discretization as the heterogeneous K realizations, with the x -direction parallel to the average groundwater flow direction. Constant hydraulic head boundary conditions were assigned at the inlet and outlet of the flow domain maintaining an average flow velocity of approximately 0.091 m/day for all realizations. All remaining boundaries were assigned as no-flow boundaries such that flow is uniform-in-the-mean. The K fields were randomly generated based on facies indicator data defined for each grid cell in T-PROGS and univariate statistics of Y (mean and variance) for each facies reported by Ramanathan et al. (2010) at different scales as shown in Table 1. These K fields were then used as input for the MODFLOW simulations. On a Core i5-1.8 GHz machine equipped with 8.00 GB of access memory, the CPU time required to solve each MODFLOW model was on the order of 10 min.

Particle tracking was employed to simulate advection, dispersion, and diffusion processes using the random walk particle tracking model (RWHet: LaBolle et al., 1996; LaBolle, 2006). RWHet is an accurate, computationally efficient particle-tracking code that has been widely used in solute transport simulations in both heterogeneous porous and fractured media (Guo et al., 2019; Reeves et al., 2008a, 2008b; Yong et al., 2008; Zhang et al., 2013). RWHet can directly read cell-by-cell flux and hydraulic head outputs generated by MODFLOW (Zhang et al., 2012), and solves the Langevin equation which is equivalent to solving the governing equation for nonreactive solute transport in saturated porous media defined as:

$$\frac{\partial}{\partial t} [\Theta(\mathbf{x}, t)c(\mathbf{x}, t)] = - \sum_{i=1}^3 \frac{\partial}{\partial x_i} [v_i(\mathbf{x}, t)\Theta(\mathbf{x}, t)c(\mathbf{x}, t)] + \sum_{i,j=1}^3 \frac{\partial}{\partial x_i} \left[D_{ij}(\mathbf{x}, t)\Theta(\mathbf{x}, t)\frac{\partial c(\mathbf{x}, t)}{\partial x_j} \right] + \sum_k q_k(\mathbf{x}, t)c_k(\mathbf{x}, t)\delta_k(\mathbf{x} - \mathbf{x}_k) \quad (1)$$

where c [M/L³] is the dissolved resident concentration; v [L/T¹] is the velocity; Θ [L³/L³] is the porosity; x_{ij} [L] is the distance along the respective Cartesian coordinate axis; c_k [M/L³] is the aqueous phase concentration in

the flux q_k [L^3/T] of water at x_k ; δ_k is a Dirac function. D_{ij} [L^2/T] is the velocity-dependent local-scale dispersion tensor defined as (Bear, 1972):

$$D_{ij} = (|\mathbf{v}| \alpha_T + D^*) \delta_{ij} + (\alpha_T - \alpha_L) v_i v_j / |\mathbf{v}| \quad (2)$$

where α_T and α_L [L] are transverse and longitudinal local dispersivities, respectively, and D^* is the molecular diffusion coefficient in the porous medium [L^2/T]. In this study, we assume $\alpha_T = \alpha_L$.

In RWHet, the concentration of the aqueous solute in a cell can be computed from the sum of particle mass $m_p(t)$ contained in that cell divided by the volume of water $\Delta V = dx \times dy \times dz$:

$$c_{ijk}(t) = \sum_{p \in V_{ijk}} m_p(t) / (\Theta \Delta V) \quad (3)$$

Readers are referred to the RWHet user manual for further information on the method and how to use it. In our study, RWHet models were parameterized with available Borden site data (e.g., Burr et al., 1994; Sudicky, 1986). Porosity (Θ) and local-scale dispersivities (α_L and α_T) were set to 0.34 and 0.0005 m, respectively, and were assumed to be isotropic and constant. The molecular diffusion coefficient in the porous formation was set to $1.166 \times 10^{-4} \text{ m}^2/\text{day}$.

We simulated mass transport through the domain following the instantaneous release of a nonreactive solute. The release time of particles at the source was 1 day and the total simulation time was 1,000 days. A rectangular contamination source (Figure S4 in Supporting Information S1) was specified to correspond with the source zone in the natural gradient tracer test at the Borden site (Sudicky, 1986) with dimensions of $3.4 < x < 6.6 \text{ m}$ ($\sim 1.5 \lambda_H$), $12 < y < 18 \text{ m}$ ($\sim 2.8 \lambda_H$), and $1.7 < z < 3.3 \text{ m}$ ($\sim 13 \lambda_V$). A total of 1 million particles were released into the source zone. Our choice of the particle number was determined based on an extensive reference to the literature of Rizzo et al. (2019), Puyguiraud et al. (2020), and Guo et al. (2019). Moreover, we found that our results including the convergence are not particle number dependent. In addition, the absorption type boundaries were used at $x = 0 \text{ m}$ and $x = 120 \text{ m}$ so that particles could leave the simulation domain at the inlet and outlet boundaries. The remaining boundaries were set as reflect boundaries so that particles will return to the domain when they reached these boundaries. Due to the 12 m ($\sim 5.7 \lambda_H$) distance between side boundaries and the source zone, and also the flow gradient from the left to the right side of the domain, we did not observe any particles reaching the side boundaries in all our realizations. Particles left the domain only if they reached the right-side boundary at $x = 120 \text{ m}$. Using the same system used to run MODFLOW simulations, the CPU time required to solve each RWHet model was generally of the order of 1 hr.

2.3. Metrics to Quantify Transport Processes

2.3.1. Solute Spreading

In a single realization of the K -field, the mass and position of all particles were used to calculate solute moments. The first moment, normalized by the mass in the solution, defines the location of the center of mass (x_c, y_c, z_c). We mainly focus on the longitudinal results here and after, so we just keep the metrics in x -direction as given by:

$$x_c(t) = \frac{1}{M_{000}} \sum_{ip=1}^{N_p} x_{ip}(t) m_{ip} \quad (4)$$

where x_{ip} is the particle position in the x -direction, m_{ip} is the mass of the particle ip , N_p is the total number of particles used in the simulation, M_{000} is the total mass of the solute. The second spatial moment defines a covariance tensor, quantifying solute spreading around the center of mass. The second centered spatial moment σ_{xx}^2 in the x -direction is defined as:

$$\sigma_{xx}^2(t) = \frac{1}{M_{000}} \sum_{ip=1}^{N_p} [x_{ip}(t)]^2 m_{ip} - x_c^2(t) \quad (5)$$

2.3.2. Effective Dispersion Coefficient

The effective dispersion coefficient (D_{xx}^{eff}) is derived from the average over the central spatial moments of the concentration field in every realization and the ensemble dispersion coefficient (D_{xx}^{ens}) is derived from the

ensemble-averaged spatial moments of whole realizations (Dagan, 1990, 1991; Dentz et al., 2000a, 2000b; Kitanidis, 1988):

$$D_{xx}^{\text{eff}}(t) = \frac{1}{2} \frac{d}{dt} \overline{\{m_{xx}^2(t) - x_c(t) x_c(t)\}} \quad (6)$$

$$D_{xx}^{\text{ens}}(t) = \frac{1}{2} \frac{d}{dt} \left\{ \overline{m_{xx}^2(t)} - \overline{x_c(t)} \cdot \overline{x_c(t)} \right\} \quad (7)$$

$$m_{xx}^2(t) = \frac{1}{M_{000}} \sum_{ip=1}^{Np} [x_{ip}(t)]^2 m_{ip} \quad (8)$$

The overbar denotes the average over the ensemble of realizations. On one hand, D_{xx}^{eff} characterizes the mean dispersion in a typical realization of an aquifer (the center-of-mass positions of the plumes in each realization are superimposed before the ensemble average is performed). On the other hand, D_{xx}^{ens} incorporates the artificial dispersion effect caused by fluctuations of the center-of-mass position of all possible dispersion properties of the subsurface environment. For additional information regarding these two definitions for the dispersion coefficient, see works by Kitanidis (1988) and Dagan (1990). The D_{xx}^{eff} converges to the asymptotic behavior of D_{xx}^{ens} (also known as the ensemble macrodispersion) at infinite times or when the solute plume samples the full heterogeneous structure of an aquifer (ergodic conditions). In practice, D_{xx}^{ens} is more commonly used in stochastic models because of its computational simplicity, regardless of whether the solute plume is ergodic or not and whether the transport time is finite or not (Dentz et al., 2000b). In addition, as mentioned above, the use of D_{xx}^{ens} inevitably introduces the artificial sample to sample fluctuations that dominate the ensemble dispersion coefficient (Dentz et al., 2000a). These lead to the overestimation of the true dispersion in the aquifer on practically relevant timescales. Thus, D_{xx}^{eff} is often more appropriate for obtaining a realistic estimate of solute transport behavior. Although de Barros and Rubin (2011) and de Barros and Dentz (2016) have quantified the uncertainty of D_{xx}^{eff} , their discussions were mainly based on a unimodal K random spatial function. In this study, we will study the temporal evolution of D_{xx}^{eff} and will quantify its uncertainty in the context of the multimodal K fields. We will further evaluate the effect of parameter variation on D_{xx}^{eff} . To better compare with previous results, the D_{xx}^{eff} is converted into effective dispersivity (α_{eff}) by dividing D_{xx}^{eff} by the average groundwater velocity of 0.091 m/day in this study.

2.3.3. Degree of Mixing

The degree of mixing provides information on the degree of homogeneity inside a solute plume in terms of how close the spatial concentration field is to its domain-averaged mean. Using the variance of the concentration field, the expression to calculate the degree of mixing (χ_ϕ) is (Amooie et al., 2017; Danckwerts, 1952):

$$\sigma_{r,\phi}^2(t) = \frac{\langle c(t)^2 \rangle - \langle c(t) \rangle^2}{\langle c(t) \rangle (c_0 - \langle c(t) \rangle)} \quad (9)$$

$$\chi_\phi(t) = 1 - \sigma_{r,\phi}^2(t) \quad (10)$$

where $\langle \cdot \rangle$ denotes spatial averaging over the domain in a single realization of the K field and c_0 is the maximum (initial) total concentration. Small values of χ_ϕ represent incomplete mixing, and as χ_ϕ approaches unity, the perfect mixing condition (i.e., $\chi_\phi = 1$ for $c(t) = \langle c(t) \rangle$) is reached.

2.3.4. Dilution Index

The dilution index $E(t)$ is a metric introduced by Kitanidis (1994) that enables the quantification of the dilution process. It is the measure of the pore volume occupied by a solute. When the solute mass distribution is discrete, this metric is expressed as:

$$E(t) = \Delta V \exp \left(- \sum_{k=1}^n P_k(t) \ln (P_k(t)) \right) \quad (11)$$

where $P_k(t)$ is the ratio of the solute mass in an elementary volume ΔV of the system to the total mass of solute in the system at time t ; n is the number of grid cells in which the solute mass is not equal to zero. $E(t)$ has dimensions

of volume. If in a continuous case, the distribution function of the mass, $p(\mathbf{x}, t)$, is introduced, which has unit of 1 over volume. It can be regarded as the probability distribution of the location of a tagged particle of the tracer at time t . By considering the continuous case as the limit of the discrete case, Equation 11 can be expressed as:

$$E(t) = \exp \left(- \int_V p(\mathbf{x}, t) \ln(p(\mathbf{x}, t)) dV \right) \quad (12)$$

$$p(\mathbf{x}, t) = \frac{c(\mathbf{x}, t)}{\int_V c(\mathbf{x}, t) dV} \quad (13)$$

where V is the total volume of the domain and $\int_V c(\mathbf{x}, t) dV$ is the total mass divided by the porosity.

Thierrin and Kitanidis (1994) reported the first estimation of $E(t)$ for the Borden tracer test data. They used an interpolation scheme to estimate the concentration at locations where measurements were not available. However, they pointed out that their interpolation may result in an overestimation of $E(t)$. Here, we recalculated $E(t)$ for the Borden data using an alternative approach proposed by de Barros et al. (2015). In this method, $P_k(t)$ is defined only for the n_p sampling points where the concentration is larger than zero:

$$P_k(t) = \frac{c_k(t) \Delta V}{n_p \Delta V c_m(t)} = \frac{c_k(t)}{n_p c_m(t)} \quad (14)$$

where:

$$c_m(t) = \sum_{k=1}^{n_p} c_k(t) / n_p \quad (15)$$

and $c_k(t)$ is the k th solute concentration measurement of the subsample of the concentration that is non-zero. The volume ΔV related to each measurement is calculated as:

$$\Delta V = \frac{M_{000}}{N c_m} \quad (16)$$

where M_{000} is the total injected mass.

2.4. Parametric Study

We considered only the scale II sedimentary architecture (i.e., bimodal M and FZ facies types) because our results discussed below (Section 3.1) show that sedimentary architecture at scale II controls the time-evolution of transport parameters studied in this work including σ_{xx}^2 , α_{eff} , χ_ϕ , and E . First, we discussed the effects of source size, local-scale dispersion, and molecular diffusion on these transport metrics. Then, we focused on sedimentary properties and K field characteristics that likely affect mass transport processes, including facies transverse mean length, volume proportion, and mean and variance of Y . For each case, the base case models and a set of 30 realizations were used to perform simulations for different parameter values, which were sufficient to show the difference in results.

The volume proportion of high-conductivity facies controls the hydrogeological system connectivity (Amooie et al., 2017; Fiori et al., 2010; Liu et al., 2020). To assess the impact of facies connectivity, the volume proportion of high permeability facies (p_M) was varied between 0.2, 0.4 (the baseline scenario), and 0.6. In this study, the K field is come up from the facies field. To further examine how the degree of K heterogeneity affects solute transport behavior, we changed the variance of $Y = \ln(K)$ (σ_Y^2) for both M and FZ facies types of scale II realizations from their original value (the baseline scenario, see Table 1) to 0 (i.e., simplified to binary model) and 1, respectively. When σ_Y^2 is equal to 0, each facies will be assigned to a constant K which is equal to the average K value and the model can be simplified to a binary model.

Given the difficulty of obtaining lithologic data in the transverse direction, an assumption is often made that lithological characteristics are isotropic in the horizontal direction (i.e., the length of facies types in transverse (y -direction) and the longitudinal (x -direction) are the same). To explore the equivalency of lithologic

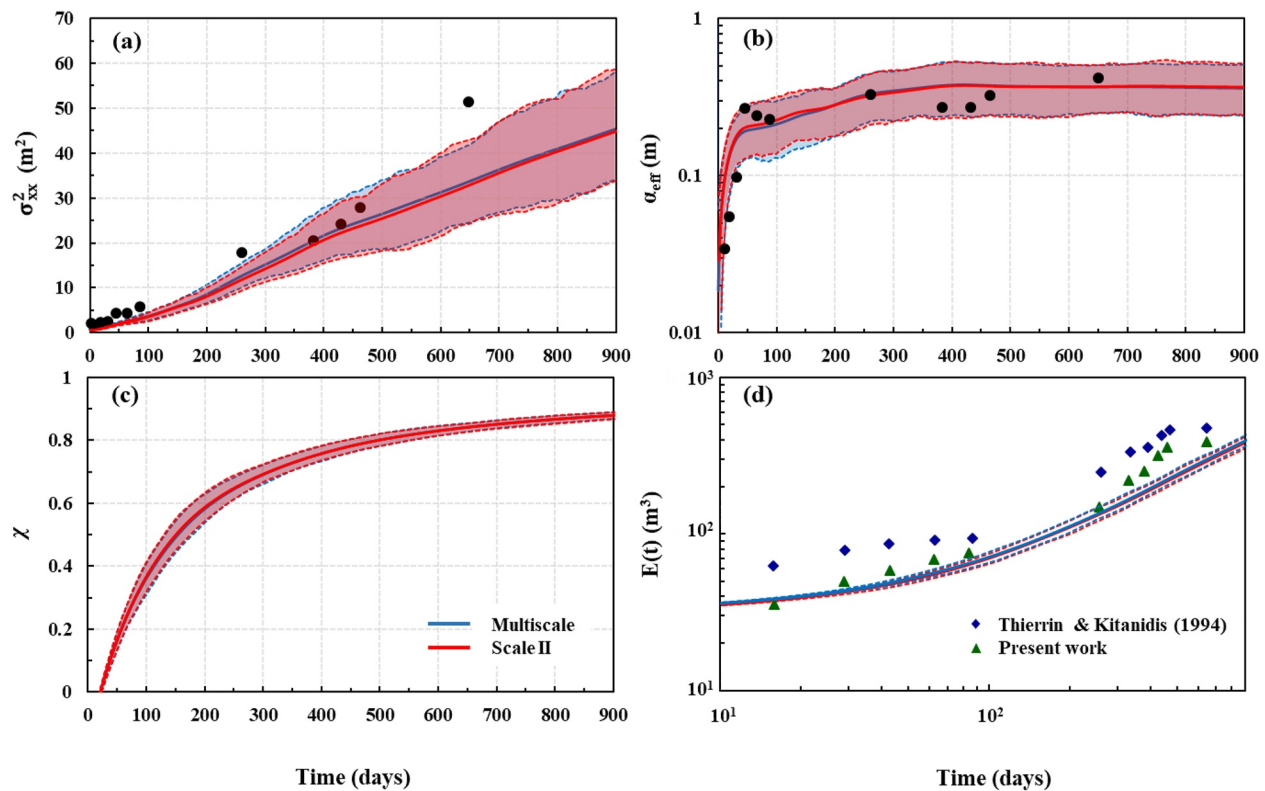


Figure 2. Simulation results of (a) second longitudinal spatial moment (σ_{xx}^2), (b) effective longitudinal dispersivity (α_{eff}), (c) degree of mixing (χ), and (d) dilution index (E). Black circles are the observed data at the Borden site reported by Freyberg (1986). Blue diamonds are the reported E data calculated by Thierrin and Kitanidis (1994). Green triangles are corrected E data using the method proposed by de Barros et al. (2015). Shaded regions (10%–90% confidence) show variabilities amongst 100 realizations with blue and red for multiscale and scale II results, respectively.

characteristics in the transverse and longitudinal directions, the transverse mean length of higher conductivity M facies was changed from 3 m in the base case scenario to 1.5 and 0.75 m without changing the longitudinal length.

At the Borden site, the geometric means of K of M and FZ facies are 7.85 and 3.38 m/day, respectively (Table 1). We define the ratio of mean conductivity as $\rho = K_M/K_{FZ}$. With increasing ρ , the contrast between the mean conductivity of the M and FZ facies increases. To examine how σ_{xx}^2 , α_{eff} , χ , and E respond to the mean conductivity ratio, we vary the magnitude of K_M while keeping K_{FZ} constant and modify the baseline scenario ($\rho \approx 2.3$) using two different ρ : 5 and 10.

3. Results and Discussion

3.1. Comparison With Field Data and Scale Relevance

We first present results for 100 models that were parameterized with available Borden data in terms of the sedimentary architecture data and the corresponding univariate statistics of Y , as discussed in Section 2.1 (see Table 1). Figure 2 shows the simulation results of the multiscale and scale II realizations about the time evolution of σ_{xx}^2 (Figure 2a), α_{eff} (Figure 2b), χ (Figure 2c), and E (Figure 2d). At a simulation time of approximately 900 days, solute particles begin leaving the domain across the open boundary downstream, which will lead to a decrease in the asymptotic values. As a result, we only show simulation results until the asymptotic values start to decrease. Under the stochastic framework, the fluctuation of the transport metrics about their ensemble mean value is a measure of the heterogeneity-introduced uncertainty (Cirpka et al., 2011; Dagan, 1990). Therefore, shaded regions with the 10%–90% confidence interval around the mean generated through 100 realizations were plotted in each panel in blue and red for multiscale and scale II cases, respectively. Figure S3 in Supporting Information S1 shows the evolution of mean and variance of the σ_{xx}^2 and α_{eff} , as well as the 95% estimated confidence intervals with the number of realizations (Ballio & Guadagnini, 2004), indicating that the 100 realizations are

sufficient to reach stable statistics. With the exception of the second moment results (Figure 2a), the observed data falls within the ensemble averages (solid lines) among 100 realizations and their range bounded by the 10th and 90th percentiles, showing a good agreement with the simulated results. Note that neither exact replication of observed conditions nor causal analysis of model discrepancies are within the scope of this article. A more detailed discussion can be found in these articles (Ramanathan et al., 2008, 2010; Ritzi et al., 2013; Soltanian, Ritzi, Dai, et al., 2015a; Soltanian et al., 2020), which indicate that the slight divergence of the simulated results from the field observations is likely attributed to variations in the simulated heterogeneity structure and release intensity as compared to field conditions during the Borden tracer test. More importantly, the tracer experiment itself represents only one realization within the domain of possible results that our stochastic models represent.

As discussed earlier, in many applications the dimensions of the source zone are comparable to the scale of heterogeneity, leading to nonergodic transport conditions. Under such conditions, dispersion and mixing are subject to uncertainty (i.e., Dentz and de Barros, 2013; Kapoor & Kitanidis, 1998; Zavala-Sanchez et al., 2009). By averaging the dispersion behavior across all 100 realizations of the K -field, we quantify the increase in σ_{xx}^2 (Figure 2a) and α_{eff} (Figure 2b) due to sediment heterogeneity. It can be seen from Figure 2 that the ensemble averages and also the 10th and 90th percentiles of scale II realizations are quite comparable to multiscale realizations for all transport processes (i.e., not much difference between blue and red curves), indicating that larger-scale facies geometries alone effectively explain dispersion properties and mixing processes. This is consistent with previous modeling studies wherein smaller-scale information within scale II contributed to only a small percentage of the transport processes. This is also consistent with prior work on ensemble dispersion using multiscale Lagrangian-based transport models (Ramanathan et al., 2010). In conclusion, for the mildly heterogeneous Borden aquifer, representing the geometries of larger-scale M and FZ facies types within flow and transport models is sufficient to explain α_{eff} and mixing.

Figure 2d shows the estimates of E provided by Thierrin and Kitanidis (1994) (blue diamonds) and corrected E estimates (green triangles) obtained following the approach described in de Barros et al. (2015). The estimation by Thierrin and Kitanidis (1994) produces higher E values caused by an interpolation effect. The corrected E values are in better agreement with our simulations, and so will be used in the rest of our analysis. The work of de Barros et al. (2015) in the Cape cod site identified different regimes for E at early, intermediate, and late simulation times. Our simulation domain and times only allowed for the study of early and intermediate time behaviors. In the early-time regime (normalized time of $(tv/\lambda_H) \ll 1$ corresponding to $t < 23$ days in our simulations) transport is mainly dominated by advection, resulting in a rapid displacement in the flow direction. The longitudinal effective dispersivity, α_{eff} increases rapidly (Figure 2b) within the early time regime, whereas E increases slightly (Figure 2d). The intermediate-time regime (normalized time of $(tv/\lambda_H) \leq 25$ corresponding to $t < 581$ days in our simulations) reflects the increasing interplay between large-scale advection and local-scale dispersion from solute injection to complete mixing. The spatial variability in K results in velocity fluctuations, which leads to strong stretching and shear deformation (de Barros et al., 2012) of the concentration field that significantly increases interfacial areas between fluids. As a result, there is an obvious increase in χ_ϕ and E (Dentz et al., 2011; Kitanidis, 1994). Sample-to-sample fluctuations in α_{eff} and χ_ϕ (shaded area) become apparent during the intermediate-time regime, reflecting the effect of spatial variability among different realizations on transport processes. However, as more sediment heterogeneity is sampled by the solute plume and as the system becomes better mixed, the fluctuations between different realizations begin to decrease (see Figure 2c) due to a reduction in variability between realizations.

The level of uncertainty in estimating σ_{xx}^2 , α_{eff} , χ_ϕ , and E are similar for scale II and multiscale realizations, further confirming that smaller-scale geometries are not as important in developing flow and transport models for the Borden tracer test. Of particular interest is the larger uncertainty (larger envelope) in metrics related to spreading (σ_{xx}^2 and α_{eff}) than those related to mixing (χ_ϕ and E). Thus, solute spreading responds more to sedimentary architecture realizations and the corresponding fluctuations of the K field than solute mixing. Solute mixing seems to be more influenced by other factors, such as molecular diffusion and local-scale dispersion, rather than the degree of heterogeneity. This confirms that if the purpose of a modeling study is to quantify dilution processes, fewer realizations of sedimentary architecture are needed. Results show that larger-scale geometries have a main controlling influence on the dilution processes. It is important to note that if one is interested in first arrival times (critical for risk analysis), then more realizations are needed to quantify uncertainty given that it is significantly affected by large-scale dispersion (Henri et al., 2016).

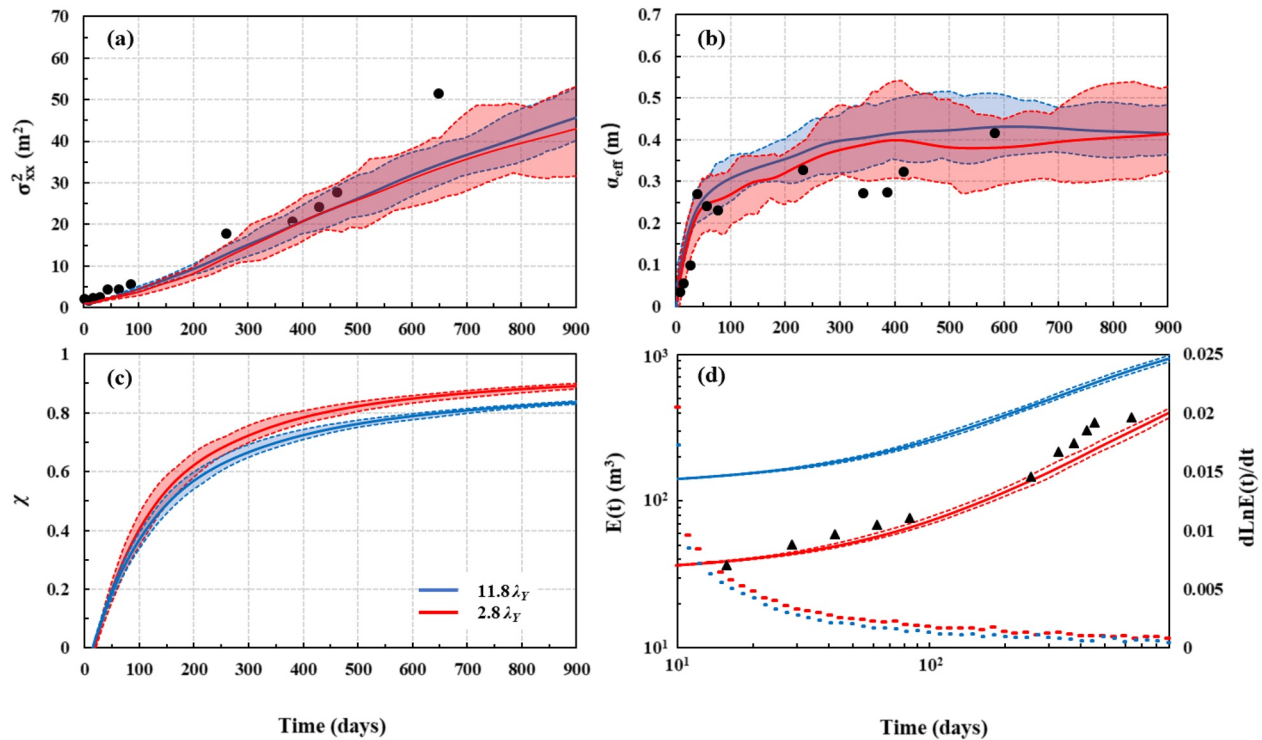


Figure 3. Effect of the source size on the results: (a) second longitudinal spatial moment (σ_{xx}^2), (b) effective longitudinal dispersivity (α_{eff}), (c) degree of mixing (χ_ϕ), and (d) dilution index (E). The source size in the y -direction is $2.8 \lambda_H$ for the small condition and $11.8 \lambda_H$ for the large condition with a fixed size in the x - and z -directions. Black circles are the observed data at the Borden site reported by Freyberg (1986). Black triangles are the corrected values based on the results from Thierrin and Kitanidis (1994). Shaded regions (10%–90% confidence) show variabilities among 30 realizations.

3.2. Effect of Source Size

By fixing the source size in the x - and z -dimensions and extending the y -dimension from 6 to 25 m (from $2.8 \lambda_H$ to about $11.8 \lambda_H$, Figure S5 in Supporting Information S1) (i.e., $2.5 < y < 27.5$ m), we investigate the results for a large source zone (relative to the log-conductivity correlation scale). In the following analysis, we will use $2.8 \lambda_H$ and $11.8 \lambda_H$ to represent small and large sources, respectively. Particles exiting the domain at the downstream boundary are primarily responsible for the decrease in transport metrics. Figure 3 shows that the uncertainty is larger in both dispersion and mixing results under the $2.8 \lambda_H$ condition. This reflects the fact that uncertainty is reduced if the solute samples more of the heterogeneity of the medium at the early stages of the transport process (i.e., a larger initial plume is closer to ergodic conditions). Although this phenomenon has been widely discussed (e.g., de Barros and Nowak, 2010; de Barros and Rubin, 2011), our new results indicate that while spreading behavior shows irregular fluctuations and large uncertainty envelopes around the mean behavior, the same is not true for mixing and dilution (Figures 3c and 3d). It can thus be inferred that the spreading process is more sensitive to the source size.

As the source size increases, the solute plume samples more of the heterogeneity of the medium, including more high- K channels. Rapid solute migration occurs along these channels, resulting in significant longitudinal dispersion. That's why α_{eff} and χ_ϕ results reflect opposite characteristics in $2.8 \lambda_H$ and $11.8 \lambda_H$. The α_{eff} is consistently higher in $11.8 \lambda_H$ (Figure 2b), while the χ_ϕ is larger for the plume size of $2.8 \lambda_H$ (Figure 2c). Figures S4 and S5 in Supporting Information S1 show the 3D and 2D (at $y = 15$ m) spatial distribution of the concentration results, respectively, under different source sizes for one scale II realization. The smaller plume has stronger horizontal and vertical deformation and more uneven concentration distribution.

It is worth noting that higher dilution index E values in Figure 3d do not indicate greater dilution for large plumes. The E is a measure of the volume occupied by the solute plume. Thus, a larger plume will necessarily have a higher E . The dotted lines in Figure 3d show the rate of increase of the logarithm of the E . Although the rate of increase is decreasing as time increases, a positive rate still indicates an increase of plume volume with time, even

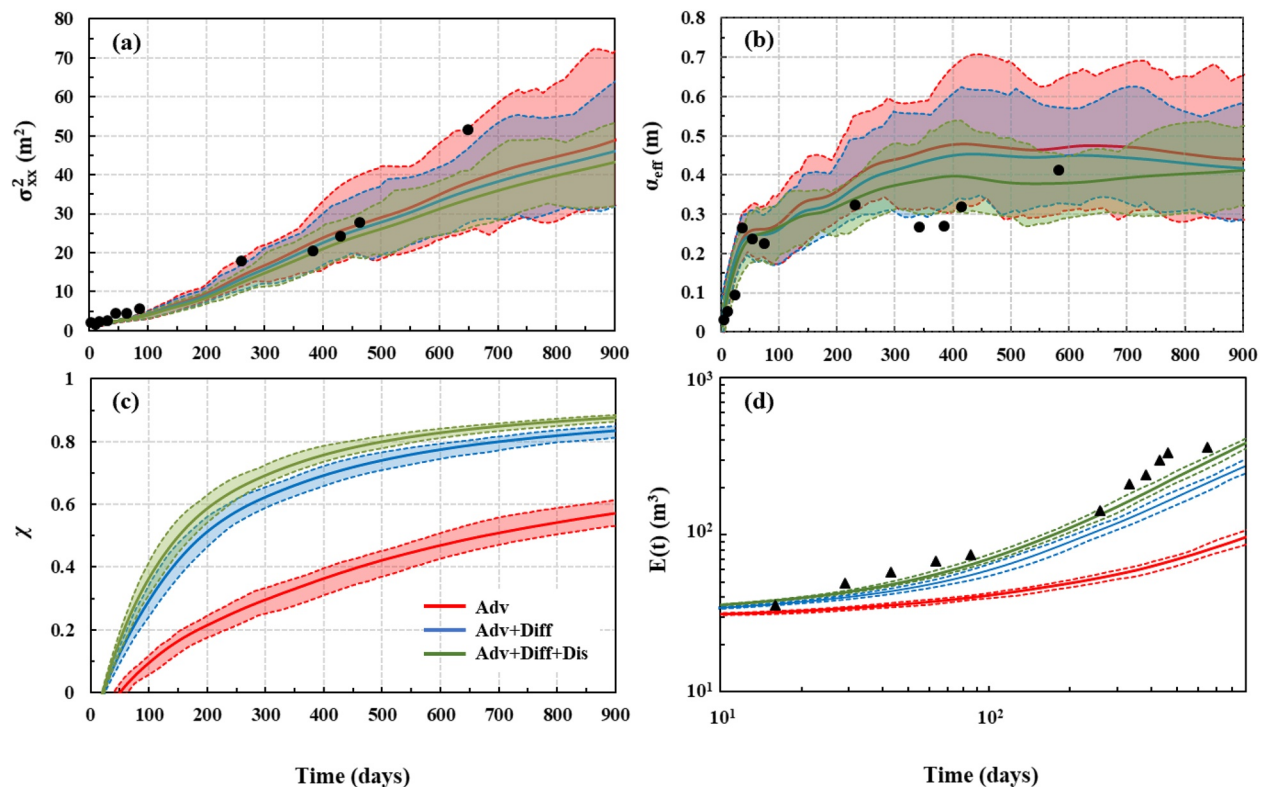


Figure 4. Effect of the local scale dispersion and molecular diffusion processes on: (a) second longitudinal spatial moment (σ_{xx}^2), (b) effective longitudinal dispersivity (α_{eff}), (c) degree of mixing (χ_ϕ), and (d) dilution index (E). Adv stands for the simulation without considering the local dispersion and molecular diffusion, Adv + Diff stands for simulation with molecular diffusion, and Adv + Diff + Dis stands for simulation with both pore scale dispersion and molecular diffusion.

if this increase is moderate. In addition, the shape of the solute plume determines the rate of increase of $\ln(E)$. A more stretched plume results in a higher rate of dilution because the mass transfer rates increase with interfacial area. As for our results, a higher rate of E is observed for the smaller source, indicating a faster dilution. This is consistent with χ_ϕ results in Figure 3c.

3.3. Effects of Local Dispersion and Molecular Diffusion

Figure 4 shows the results with and without local-scale dispersion and molecular diffusion. Here, “Adv” is used to stand for the simulations without considering the local-scale dispersion and diffusion.

As expected, the results illustrate that both local-scale dispersion and molecular diffusion lead to a large increase in mixing and a decrease in large-scale dispersion (Figure 4). The physical processes lead to a reduction in the uncertainty of the model output when compared to simulations under pure advection. Among these results, large-scale solute dispersion showed greater sensitivity to local-scale dispersion (see Figures 4a and 4b), while molecular diffusion had a greater impact on solute mixing (Figures 4c and 4d). This significant effects of molecular diffusion on mixing can be attributed to the presence of regions of low flow rates within the aquifer. These results are in agreement with previous findings in the literature (Cirpka et al., 2011; Rolle et al., 2012; Szic et al., 2013). Contrasts in the conductivity field, and consequently flow variability, leads to enhanced solute mixing. As for the output uncertainty, the enhanced dilution contributed by local-scale dispersion and diffusion helps in reducing the sample-to-sample fluctuations (i.e., conductivity realizations) of the concentration field and therefore, uncertainty in large-scale spreading is reduced (see details in Dentz and de Barros, 2013). Juxtaposition of Figures 3 and 4 indicate that transport is more sensitive to local-scale dispersion and diffusion rather than the source size (for the range of parameters explored).

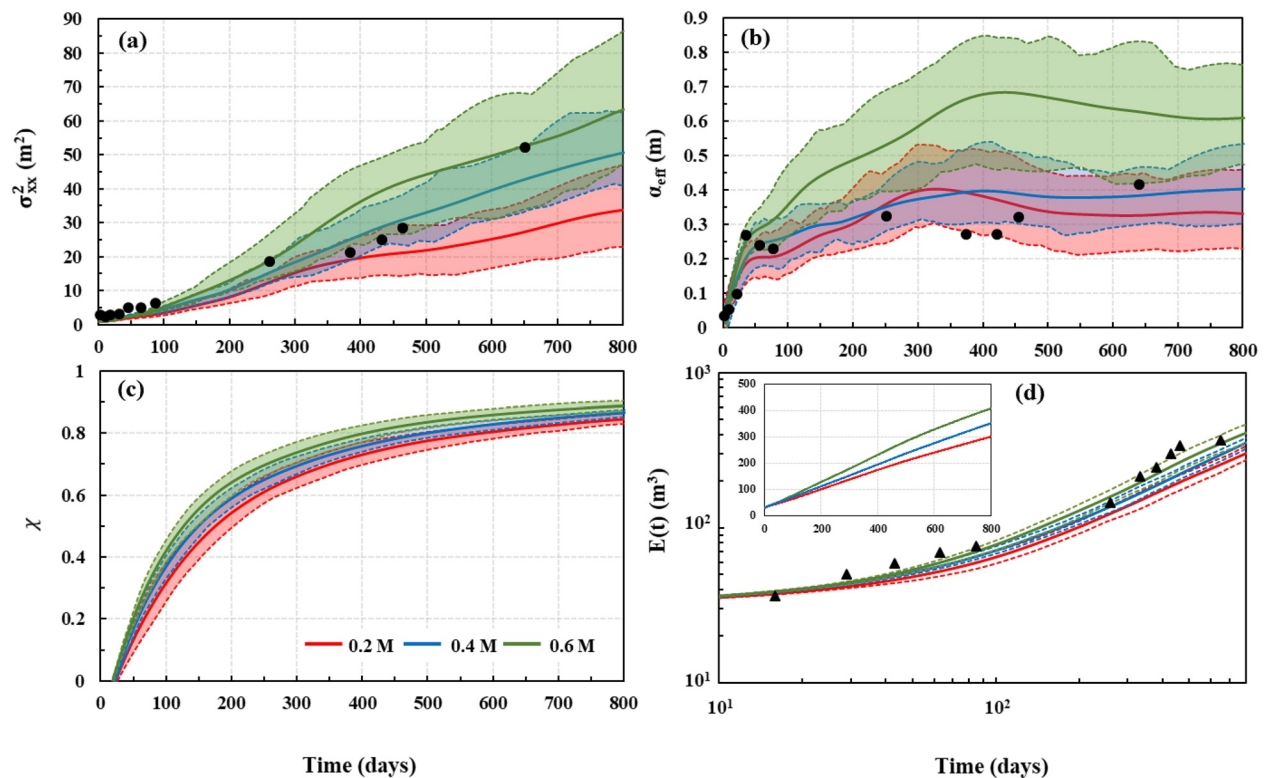


Figure 5. Effect of the volume proportion of M facies type on: (a) second longitudinal spatial moment (σ_{xx}^2), (b) effective longitudinal dispersivity (α_{eff}), (c) degree of mixing (χ_ϕ), and (d) dilution index (E). The 0.4 volume proportion is the observed volume proportion of M facies types at the Borden site.

3.4. Effect of Geologic Structure and Univariate Statistics

3.4.1. Facies Volume Proportion

The volume proportion of facies types controls connectivity, with larger proportions of M facies types increasing the connectivity of preferential flow pathways, resulting in increased velocity variance (Harter, 2005; Pescimoro et al., 2019; Pryshlak et al., 2015; Soltanian et al., 2020). Simulation results show that increasing p_M enhances both dispersion and mixing processes (Figure 5). At 60% p_M , particles begin leaving the domain after roughly 800 days. Although the overall spatial statistical properties of the Y field remain the same in our three scenarios (e.g., mean and variance), the difference in the correlation structure significantly alters the temporal and spatial distribution of the concentration. Under the large p_M condition (0.6 M), the so-called channeling effect involves a larger velocity variability (Gotovac et al., 2009; Janković et al., 2003). Solutes rapidly pass through narrow channels with a large longitudinal correlation length, resulting in enhanced dispersion (Figures 5a and 5b). As the plume deforms, contact between the plume and the surrounding fluid increases, and the increased concentration gradient further enhances χ_ϕ (Figure 5c). However, the wider plume distribution also increases the concentration uncertainty at the plume boundary between realizations, resulting in a significant increase in the uncertainty of σ_{xx}^2 and α_{eff} as p_M increases. Again, χ_ϕ and E are less sensitive to proportion changes. Since the difference of the average E is not obvious in the semi-log coordinate, an inset with regular coordinates is added for better comparison (same in Figure 6d below).

Soltanian et al. (2020) developed a new semi-analytical solution in a Lagrangian framework to quantify the dilution index E of solute plumes in geological formations displaying multiscale sedimentary architecture. They found that dilution is significantly enhanced as p_M increases from 0.1 to 0.2, but only a slight increase in E was observed as p_M continued to increase to 0.6. They interpreted this as no significant change in the difference between the longitudinal trajectory covariance and cross-covariance, which is the main contributor to the dilution when increasing p_M from 0.2 to 0.6. Therefore, based on their conclusions, given the strong influence of high- K facies on transport processes, slight volume changes may lead to significant differences in solute dispersion and mixing when their volume proportions are inherently low.

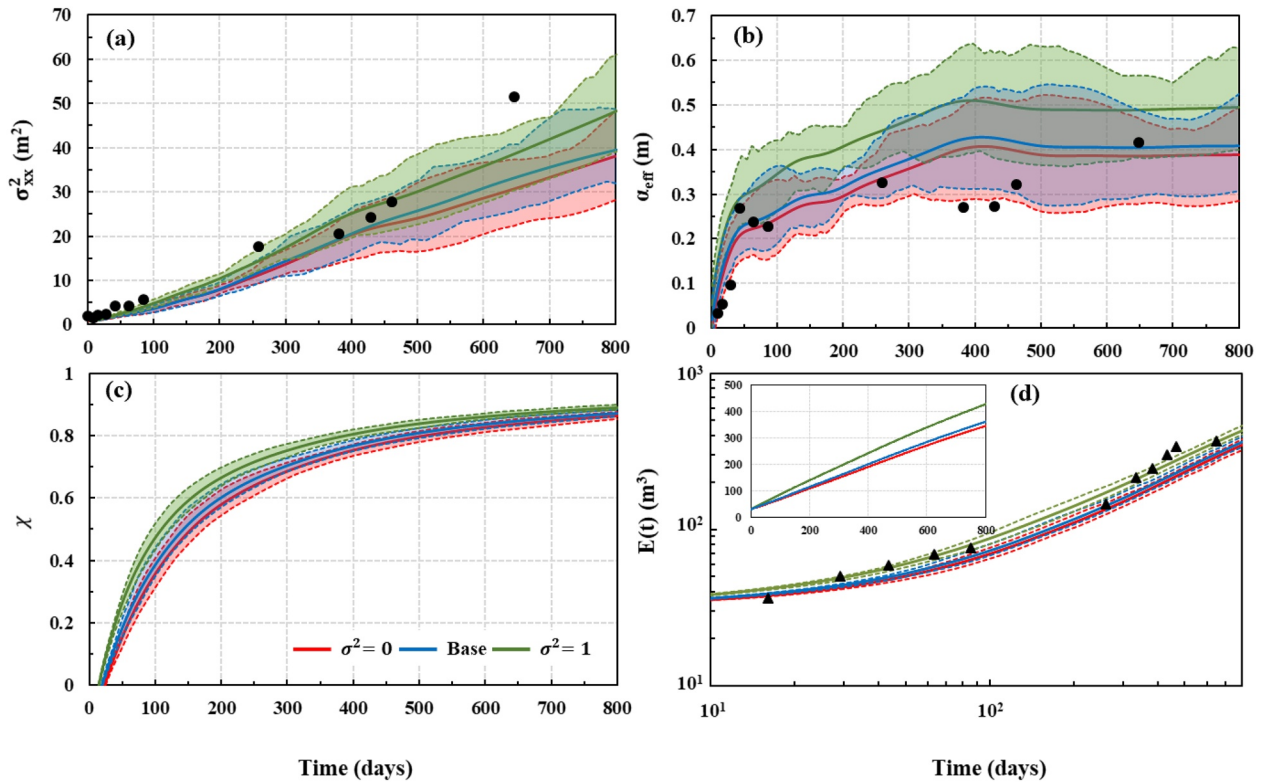


Figure 6. Effect of the σ_y^2 of M and FZ facies types on: (a) second longitudinal spatial moment (σ_{xx}^2), (b) effective longitudinal dispersivity (α_{eff}), (c) degree of mixing (χ_ϕ), and (d) dilution index (E).

3.4.2. Hydraulic Conductivity Variance

We performed the simulation by using scale II realizations with different K variances to explore the effects of the degree of heterogeneity on mixing and spreading (Figure 6). Higher heterogeneity, manifested through a larger σ_y^2 , enhances dispersion and mixing. The results indicate that even for our mildly heterogeneous medium ($\sigma_y^2 \leq 1$), the enhancement is significant. The uncertainty of α_{eff} and χ_ϕ remains constant with increasing degrees of heterogeneity. Although our results have already indicated that large-scale heterogeneity controls the plume transport (Figure 2), conductivity variability within the facies is still needed to accurately represent the transport behavior. When conductivity variability is removed (the variance of K is zero), the σ_{xx}^2 , α_{eff} , χ_ϕ , and E results produce an underestimation of nearly 10% over long transport times.

3.4.3. Facies Transverse Mean Length

The influence of transverse lithofacies mean length (y-direction) on transport processes is shown in Figure 7, which indicates that variations in the transverse mean length have a very weak influence on σ_{xx}^2 , α_{eff} , χ_ϕ , and E . Generally, changing transverse facies mean length will inevitably change the migration path of the plume in the horizontal direction. For example, when the length in the y-direction decreases, the solute will travel more in the x-direction, which should lead to an increase in longitudinal dispersion and transverse mixing. But this kind of change is not obvious (Figures 7b and 7c). On the other hand, while the averages of these transport quantities are identical, their fluctuation behavior is found to be different. As the transverse mean length increases, uncertainty in both dispersion and mixing slightly increases, but this kind of change is relatively negligible compared to those caused by the other more sensitive parameters. Thus, the transverse mean length does not significantly affect solute spreading or mixing, and the main flow direction information is the most important to explain the plume dynamics.

3.4.4. Mean Difference in Hydraulic Conductivity

The K distribution in our simulations depends on the facies distribution, as explained in Section 2.2. For a given heterogeneity realization, the randomly generated K fields are different. Therefore, we selected one facies distri-

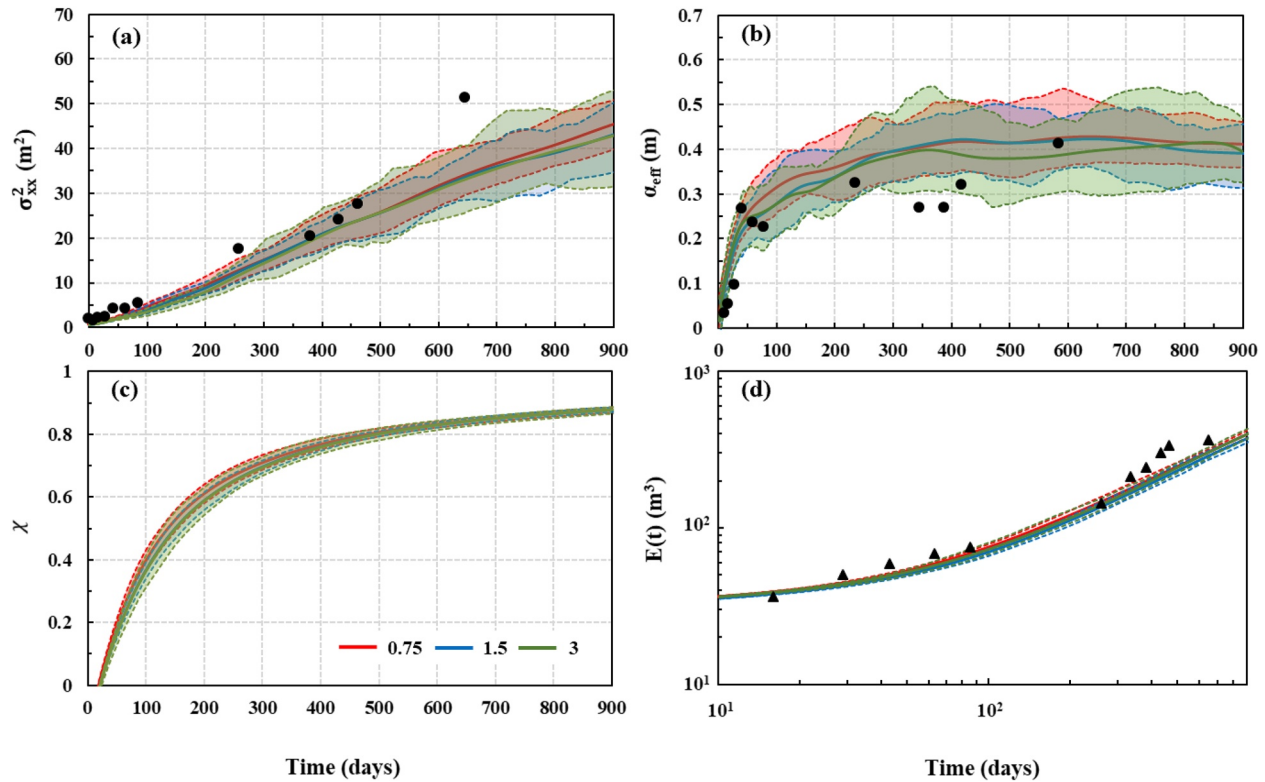


Figure 7. Effect of the transverse mean length of M facies type on: (a) second longitudinal spatial moment (σ_{xx}^2), (b) effective longitudinal dispersivity (α_{eff}), (c) degree of mixing (χ_ϕ), and (d) dilution index (E). The l_r of 3 m is the observed mean length for M facies types in the Borden site.

bution realization at scale II and randomly generated 30 different K fields for different ρ values. In addition, to show that consistency among geologic realizations, we supplemented results of five additional geologic realizations (in Figure S6 in Supporting Information S1).

As can be seen from the results shown in Figure 8, the contrast in mean conductivity is one of the most influential parameters controlling solute transport. All the transport metrics increase as the mean conductivity contrast increases. When ρ is 10, the particles start to leave the downstream boundary after roughly 250 days and all particles leave the domain after approximately 900 days. Changes are most pronounced in σ_{xx}^2 , which increases by up to 15 times as ρ increases from 2.3 to 10 (Figure 8a). It has been known that the flow variability in heterogeneous formations is mainly manifested in flow focusing in high-conductivity and defocusing in low-conductivity inclusions (Cirpka et al., 2011; Werth et al., 2006). When ρ is 10, χ_ϕ increases to 90% in roughly 200 days, five times earlier than the required time in the baseline scenario. By modeling an idealized porous medium with high- K inclusions, Werth et al. (2006) found that the time required for mixing and reactions was reduced by flow focusing in the vicinity of high- K zones, thereby enhancing transverse mixing. These patterns were experimentally supported by Bauer et al. (2009) and Rolle et al. (2009). Results also show that there are small differences between 30 K models of a given realization with different ρ (with almost no envelopes). This reflects the stronger control of solute transport by the sedimentary architecture than in facies variation in K . This is also verified by the use of five geologic realizations in Figure S6 in Supporting Information S1. Though there is variability amongst geologic models, the time evolution patterns of solute mixing and dispersion are consistent. Similarly, solute dispersion shows greater fluctuations compared to solute mixing.

4. Conclusions

This study explored the behavior of nonreactive solutes in multiscale heterogeneous geological media and evaluated the influence of various parameters on the different solute spreading and mixing metrics. Spreading was

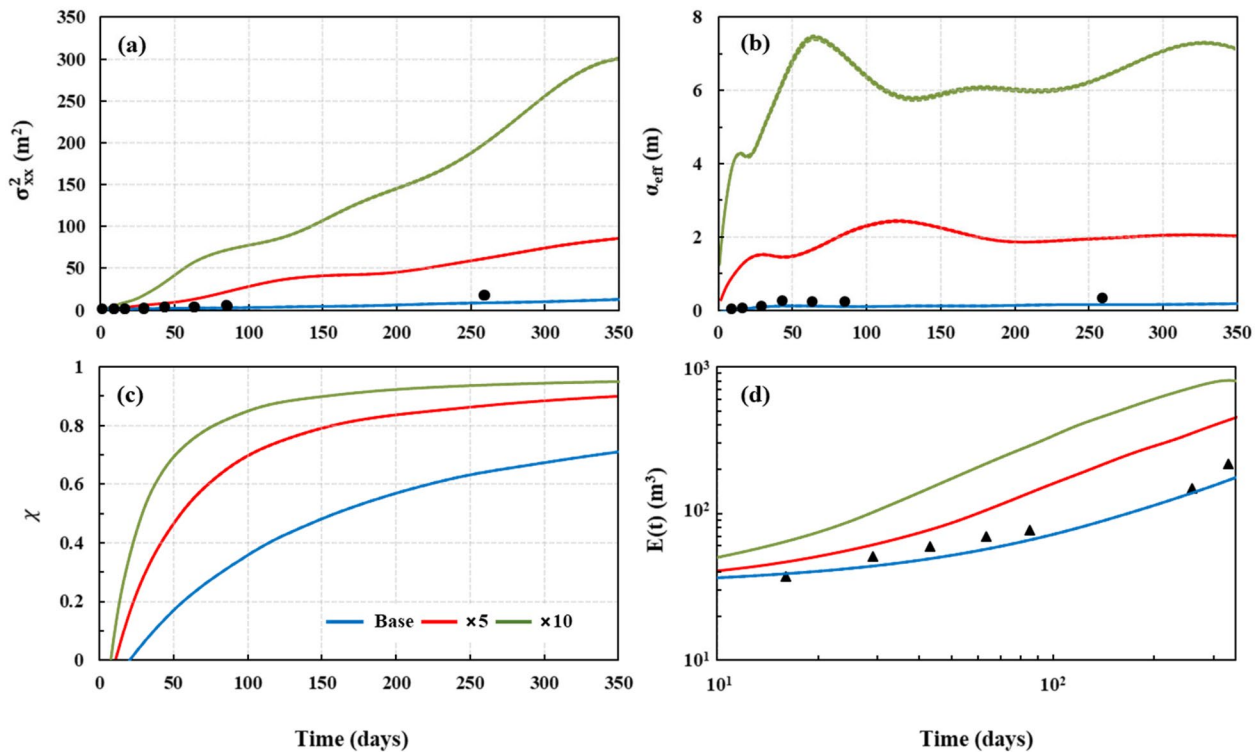


Figure 8. Effect of the ratio of M facies to FZ facies mean conductivity (ρ) on: (a) second longitudinal spatial moment (σ_{xx}^2), (b) effective longitudinal dispersivity (α_{eff}), (c) degree of mixing (χ_ϕ), and (d) dilution index (E).

quantified by the second moment of the normalized spatial solute concentration distribution and the effective dispersion. Mixing was quantified by the degree of mixing and the dilution index.

Our results indicate that the initial plume size, molecular diffusion, and local-scale dispersion have significant effects on solute spreading and mixing. The use of a smaller plume size (relative to the log-conductivity correlation length) will lead to a significant increase in the uncertainty of the simulation results, a slight decrease in solute dispersion, and a slight increase in solute mixing. But overall, for the scenarios investigated in this work, the effect of the initial plume size relative to the correlation length is relatively limited. The effects of molecular diffusion, as well as local-scale dispersion, lead to a significant enhancement of solute mixing, effectively reduce the uncertainty of simulation results, and also correct the overestimation error of solute dispersion. In contrast to solute dispersion, solute mixing seems to be influenced more by molecular diffusion and local-scale dispersion.

For the range of parameters (sediment attributes and facies-scale univariate statistics) investigated in this work, our results indicate that small-scale (level I) structural information has no significant impact on solute transport, while larger-scale (level II) stratal units control plume spreading. As noted by Dai et al. (2004) and Soltanian and Ritzi (2014), the classification of lithofacies is not unique, there is no definite answer on how to define the facies types at each scale and, as a result, which scale structure has a controlling influence on solute transport. However, the insight into the relationship between the heterogeneous sedimentary structure of each scale with solute dispersion and mixing gives us strong support for heterogeneous structures simplification and model parameterization reduction.

In this article, we explore for the first time the effect of transverse lithofacies mean length (y-direction) on solute transport, and the results show that the main flow direction (x-direction) information is the most important to explain the plume dynamics. In addition, large volume proportion of high permeability facies (which means high connectivity), high heterogeneity, and high hydraulic conductivity contrast all lead to significant enhancement of longitudinal dispersion and transverse mixing. Among them, the increase of connectivity also leads to the increase of model uncertainty, and the change of heterogeneity hardly affects the uncertainty. In this article, the

dilution index of the Borden site is recalculated by introducing the calculation method of de Barros et al. (2015). The corrected dilution index values are in better agreement with our simulation results.

Furthermore, when we compare all the results together, an interesting result is found that solute spreading appears to be more responsive to sedimentary architecture realizations and the corresponding fluctuations of the K field than solute mixing. This finding can provide thinking for modelers: heterogeneous structure realizations need to be constructed according to the purpose of modeling research. When the purpose is to quantify the dilution processes, it can use fewer realizations of sedimentary architecture. Whereas, if risk analysis is performed, more realizations are needed to quantify the uncertainty given that it is significantly affected by large-scale dispersion.

Based on these results, a future possible extension of this work would be to examine multiscale dispersion and mixing processes in the context of reactive solute transport to parse the relative influence of heterogeneity scales on both mixing (as performed in this study) and nutrient transformations. Previous studies have shown that microbial reaction rates are often greatest where complementary solutes are mixed most efficiently (e.g., Chu et al., 2005; Stegen et al., 2016), which exist in both the multiscale and scale II conditions. Given that larger-scale II heterogeneity alone is sufficient to effectively represent the dispersion properties, the general distribution of reaction zones throughout the subsurface is likely similarly well-represented solely by scale II structures. Often conditions for efficient microbial reactions are subject to small-scale variations in facies types, however, especially regarding spatial variations in electron donors (e.g., dissolved organic carbon) which are often autochthonously sourced from organic-rich sediments. As result, the regions of enhanced microbial activity tend to exhibit high spatial heterogeneity and vary with facies type, so multiscale conditions may be necessary to accurately characterize their distribution throughout the subsurface.

Data Availability Statement

The observation data of the Borden tracer test is available from (Freyberg, 1986, <https://doi.org/10.1029/WR022i013p02031>). The measured data for modeling the sedimentary architecture is available from (Ramanathan et al., 2010, <https://doi.org/10.1029/2009WR007810>; Ritzi et al., 2013, <https://doi.org/10.1002/wrcr.20165>).

Acknowledgments

This work is funded by the National Key R&D Program of China (No.2018YFC1800904), the National Natural Science Foundation of China (NSFC: 42141011, 42002254).

References

- Amooie, M. A., Soltanian, M. R., Xiong, F., Dai, Z., & Moortgat, J. (2017). Mixing and spreading of multiphase fluids in heterogeneous bimodal porous media. *Geomechanics and Geophysics for Geo-Energy and Geo-Resources*, 3(3), 225–244. <https://doi.org/10.1007/s40948-017-0060-8>
- Anderson, M. P., & McCray, J. (2011). Foreword: Lessons learned about contaminant hydrogeology from legacy research sites. *Groundwater*, 49(5), 617–619. <https://doi.org/10.1111/j.1745-6584.2011.00842.x>
- Attinger, S., Dentz, M., Kinzelbach, H., & Kinzelbach, W. (1999). Temporal behavior of a solute cloud in a chemically heterogeneous porous medium. *Journal of Fluid Mechanics*, 386, 77–104. <https://doi.org/10.1017/s0022112099004334>
- Attinger, S., Dentz, M., & Kinzelbach, W. (2004). Exact transverse macro dispersion coefficients for transport in heterogeneous porous media. *Stochastic Environmental Research and Risk Assessment*, 18(1), 9–15. <https://doi.org/10.1007/s00477-003-0160-6>
- Ballio, F., & Guadagnini, A. (2004). Convergence assessment of numerical Monte Carlo simulations in groundwater hydrology. *Water Resources Research*, 40(4). <https://doi.org/10.1029/2003wr002876>
- Bauer, R. D., Rolle, M., Bauer, S., Eberhardt, C., Grathwohl, P., Kolditz, O., et al. (2009). Enhanced biodegradation by hydraulic heterogeneities in petroleum hydrocarbon plumes. *Journal of Contaminant Hydrology*, 105(1–2), 56–68. <https://doi.org/10.1016/j.jconhyd.2008.11.004>
- Bear, J. (1972). *Dynamics of fluids in porous media*. Elsevier.
- Bellin, A., Rubin, Y., & Rinaldo, A. (1994). Eulerian-Lagrangian approach for modeling of flow and transport in heterogeneous geological formations. *Water Resources Research*, 30(11), 2913–2924. <https://doi.org/10.1029/94wr01489>
- Bianchi, M., Zheng, C., Wilson, C., Tick, G. R., Liu, G., & Gorelick, S. M. (2011). Spatial connectivity in a highly heterogeneous aquifer: From cores to preferential flow paths. *Water Resources Research*, 47(5). <https://doi.org/10.1029/2009wr008966>
- Burr, D. T., Sudicky, E. A., & Naff, R. L. (1994). Nonreactive and reactive solute transport in three-dimensional heterogeneous porous media: Mean displacement, plume spreading, and uncertainty. *Water Resources Research*, 30(3), 791–815. <https://doi.org/10.1029/93wr02946>
- Carle, S. F. (1999). *T-PROGS: Transition probability geostatistical software, Version 2.1*. Department of Land, Air and Water Resources, University of California.
- Chu, M., Kitanidis, P. K., & McCarty, P. L. (2005). Modeling microbial reactions at the plume fringe subject to transverse mixing in porous media: When can the rates of microbial reaction be assumed to be instantaneous? *Water Resources Research*, 41(6). <https://doi.org/10.1029/2004wr003495>
- Cirpka, O. A., de Barros, F. P., Chiogna, G., Rolle, M., & Nowak, W. (2011). Stochastic flux-related analysis of transverse mixing in two-dimensional heterogeneous porous media. *Water Resources Research*, 47(6). <https://doi.org/10.1029/2010wr010279>
- Dagan, G. (1984). Solute transport in heterogeneous porous formations. *Journal of Fluid Mechanics*, 145, 151–177. <https://doi.org/10.1017/s0022112084002858>
- Dagan, G. (1988). Time-dependent macrodispersion for solute transport in anisotropic heterogeneous aquifers. *Water Resources Research*, 24(9), 1491–1500. <https://doi.org/10.1029/wr024i009p01491>
- Dagan, G. (1989). *Flow and transport in porous formations*. Springer Science & Business Media.

- Dagan, G. (1990). Transport in heterogeneous porous formations: Spatial moments, ergodicity, and effective dispersion. *Water Resources Research*, 26(6), 1281–1290. <https://doi.org/10.1029/wr026i006p01281>
- Dagan, G. (1991). Dispersion of a passive solute in non-ergodic transport by steady velocity fields in heterogeneous formations. *Journal of Fluid Mechanics*, 233, 197–210. <https://doi.org/10.1017/s0022112091000459>
- Dai, Z., Ritzi, R. W., Jr., Huang, C., Rubin, Y. N., & Dominic, D. F. (2004). Transport in heterogeneous sediments with multimodal conductivity and hierarchical organization across scales. *Journal of Hydrology*, 294(1–3), 68–86. <https://doi.org/10.1016/j.jhydrol.2003.10.024>
- Dai, Z., Stauffer, P. H., Carey, J. W., Middleton, R. S., Lu, Z., Jacobs, J. F., et al. (2014). Pre-site characterization risk analysis for commercial-scale carbon sequestration. *Environmental Science & Technology*, 48(7), 3908–3915. <https://doi.org/10.1021/es405468p>
- Dai, Z., Zhan, C., Dong, S., Yin, S., Zhang, X., & Soltanian, M. R. (2020). How does resolution of sedimentary architecture data affect plume dispersion in multiscale and hierarchical systems? *Journal of Hydrology*, 582, 124516. <https://doi.org/10.1016/j.jhydrol.2019.124516>
- Dai, Z., Zhan, C., Soltanian, M. R., Ritzi, R. W., & Zhang, X. (2019). Identifying spatial correlation structure of multimodal permeability in hierarchical media with Markov chain approach. *Journal of Hydrology*, 568, 703–715. <https://doi.org/10.1016/j.jhydrol.2018.11.032>
- Dai, Z., Zhang, Y., Bielicki, J., Amooie, M. A., Zhang, M., Yang, C., et al. (2018). Heterogeneity-assisted carbon dioxide storage in marine sediments. *Applied Energy*, 225, 876–883. <https://doi.org/10.1016/j.apenergy.2018.05.038>
- Danckwerts, P. V. (1952). The definition and measurement of some characteristics of mixtures. *Applied Scientific Research, Section A*, 3(4), 279–296. <https://doi.org/10.1007/bf03184936>
- de Barros, F. P., & Dentz, M. (2016). Pictures of blockscale transport: Effective versus ensemble dispersion and its uncertainty. *Advances in Water Resources*, 91, 11–22. <https://doi.org/10.1016/j.advwatres.2016.03.004>
- de Barros, F. P., Dentz, M., Koch, J., & Nowak, W. (2012). Flow topology and scalar mixing in spatially heterogeneous flow fields. *Geophysical Research Letters*, 39(8). <https://doi.org/10.1029/2012gl051302>
- de Barros, F. P., & Nowak, W. (2010). On the link between contaminant source release conditions and plume prediction uncertainty. *Journal of Contaminant Hydrology*, 116(1–4), 24–34. <https://doi.org/10.1016/j.jconhyd.2010.05.004>
- de Barros, F. P., & Rubin, Y. (2011). Modelling of block-scale macrodispersion as a random function. *Journal of Fluid Mechanics*, 676, 514–545. <https://doi.org/10.1017/jfm.2011.65>
- de Barros, F. P. J., Fiori, A., Boso, F., & Bellin, A. (2015). A theoretical framework for modeling dilution enhancement of non-reactive solutes in heterogeneous porous media. *Journal of Contaminant Hydrology*, 175, 72–83. <https://doi.org/10.1016/j.jconhyd.2015.01.004>
- Dentz, M., & de Barros, F. P. (2013). Dispersion variance for transport in heterogeneous porous media. *Water Resources Research*, 49(6), 3443–3461. <https://doi.org/10.1002/wrcr.20288>
- Dentz, M., de Barros, F. P., Le Borgne, T., & Lester, D. R. (2018). Evolution of solute blobs in heterogeneous porous media. *Journal of Fluid Mechanics*, 853, 621–646. <https://doi.org/10.1017/jfm.2018.588>
- Dentz, M., Kinzelbach, H., Attinger, S., & Kinzelbach, W. (2000a). Temporal behavior of a solute cloud in a heterogeneous porous medium: 1. Point-like injection. *Water Resources Research*, 36(12), 3591–3604. <https://doi.org/10.1029/2000wr900162>
- Dentz, M., Kinzelbach, H., Attinger, S., & Kinzelbach, W. (2000b). Temporal behavior of a solute cloud in a heterogeneous porous medium: 2. Spatially extended injection. *Water Resources Research*, 36(12), 3605–3614. <https://doi.org/10.1029/2000wr900211>
- Dentz, M., Le Borgne, T., Englert, A., & Bijeljic, B. (2011). Mixing, spreading and reaction in heterogeneous media: A brief review. *Journal of Contaminant Hydrology*, 120, 1–17. <https://doi.org/10.1016/j.jconhyd.2010.05.002>
- Di Dato, M., de Barros, F. P., Fiori, A., & Bellin, A. (2016). Effects of the hydraulic conductivity microstructure on macrodispersivity. *Water Resources Research*, 52(9), 6818–6832. <https://doi.org/10.1002/2016wr019086>
- Ershadnia, R., Hajirezaie, S., Amooie, A., Wallace, C. D., Gershenson, N. I., Hosseini, S. A., et al. (2021). CO₂ geological sequestration in multiscale heterogeneous aquifers: Effects of heterogeneity, connectivity, impurity, and hysteresis. *Advances in Water Resources*, 151, 103895. <https://doi.org/10.1016/j.advwatres.2021.103895>
- Ershadnia, R., Wallace, C. D., Hosseini, S. A., Dai, Z., & Soltanian, M. R. (2021). Capillary heterogeneity linked to methane lateral migration in shallow unconfined aquifers. *Geophysical Research Letters*, 48(23), e2021GL095685. <https://doi.org/10.1029/2021gl095685>
- Fiori, A. (2001). On the influence of local dispersion in solute transport through formations with evolving scales of heterogeneity. *Water Resources Research*, 37(2), 235–242. <https://doi.org/10.1029/2000wr900245>
- Fiori, A., Boso, F., de Barros, F. P., De Bartolo, S., Frampton, A., Severino, G., et al. (2010). An indirect assessment on the impact of connectivity of conductivity classes upon longitudinal asymptotic macrodispersivity. *Water Resources Research*, 46(8). <https://doi.org/10.1029/2009wr008590>
- Fiori, A., & Dagan, G. (1999). Concentration fluctuations in transport by groundwater: Comparison between theory and field experiments. *Water Resources Research*, 35(1), 105–112. <https://doi.org/10.1029/98wr01862>
- Fiori, A., & Dagan, G. (2000). Concentration fluctuations in aquifer transport: A rigorous first-order solution and applications. *Journal of Contaminant Hydrology*, 45(1–2), 139–163. [https://doi.org/10.1016/s0169-7722\(00\)00123-6](https://doi.org/10.1016/s0169-7722(00)00123-6)
- Freyberg, D. L. (1986). A natural gradient experiment on solute transport in a sand aquifer: 2. Spatial moments and the advection and dispersion of nonreactive tracers. *Water Resources Research*, 22(13), 2031–2046. <https://doi.org/10.1029/wr022i013p02031>
- Gelhar, L. W. (1986). Stochastic subsurface hydrology from theory to applications. *Water Resources Research*, 22(9S), 135S–145S. <https://doi.org/10.1029/wr022i09sp0135s>
- Gelhar, L. W., & Axness, C. L. (1983). Three-dimensional stochastic analysis of macrodispersion in aquifers. *Water Resources Research*, 19(1), 161–180. <https://doi.org/10.1029/wr019i001p0161>
- Gotovac, H., Cvetkovic, V., & Andricevic, R. (2009). Flow and travel time statistics in highly heterogeneous porous media. *Water Resources Research*, 45(7). <https://doi.org/10.1029/2008wr007168>
- Guo, Z., Fogg, G. E., Brusseau, M. L., LaBolle, E. M., & Lopez, J. (2019). Modeling groundwater contaminant transport in the presence of large heterogeneity: A case study comparing MT3D and RWHE. *Hydrogeology Journal*, 27(4), 1363–1371. <https://doi.org/10.1007/s10040-019-01938-9>
- Harbaugh, A. W. (2005). *MODFLOW-2005, the US Geological Survey modular ground-water model: The ground-water flow process* (pp. 6–A16). US Department of the Interior, US Geological Survey.
- Harter, T. (2005). Finite-size scaling analysis of percolation in three-dimensional correlated binary Markov chain random fields. *Physical Review E*, 72(2), 026120. <https://doi.org/10.1103/physreve.72.026120>
- Henri, C. V., Fernández-García, D., & De Barros, F. P. (2016). Assessing the joint impact of DNAPL source-zone behavior and degradation products on the probabilistic characterization of human health risk. *Advances in Water Resources*, 88, 124–138. <https://doi.org/10.1016/j.advwatres.2015.12.012>
- Janković, I., Fiori, A., & Dagan, G. (2003). Flow and transport in highly heterogeneous formations: 3. Numerical simulations and comparison with theoretical results. *Water Resources Research*, 39(9). <https://doi.org/10.1029/2002WR001721>

- Jha, B., Cueto-Felgueroso, L., & Juanes, R. (2011). Fluid mixing from viscous fingering. *Physical Review Letters*, 106(19), 194502. <https://doi.org/10.1103/physrevlett.106.194502>
- Jiménez-Martínez, J., Anna, P. D., Tabuteau, H., Turuban, R., Borgne, T. L., & Méheust, Y. (2015). Pore-scale mechanisms for the enhancement of mixing in unsaturated porous media and implications for chemical reactions. *Geophysical Research Letters*, 42(13), 5316–5324. <https://doi.org/10.1002/2015GL064513>
- Kapoor, V., & Kitanidis, P. K. (1998). Concentration fluctuations and dilution in aquifers. *Water Resources Research*, 34(5), 1181–1193. <https://doi.org/10.1029/97wr03608>
- Kitanidis, P. K. (1988). Prediction by the method of moments of transport in a heterogeneous formation. *Journal of Hydrology*, 102(1–4), 453–473. [https://doi.org/10.1016/0022-1694\(88\)90111-4](https://doi.org/10.1016/0022-1694(88)90111-4)
- Kitanidis, P. K. (1994). The concept of the dilution index. *Water Resources Research*, 30(7), 2011–2026. <https://doi.org/10.1029/94wr00762>
- Kitanidis, P. K., & McCarty, P. L. (Eds.) (2012). *Delivery and mixing in the subsurface: Processes and design principles for in situ remediation* (Vol. 4). Springer Science & Business Media.
- LaBolle, E. M. (2006). RWHet: Random Walk Particle Model for simulating transport in heterogeneous permeable media, version 3.2. In *User's manual and program documentation*. University of California.
- LaBolle, E. M., Fogg, G. E., & Tompson, A. F. (1996). Random-walk simulation of transport in heterogeneous porous media: Local mass-conservation problem and implementation methods. *Water Resources Research*, 32(3), 583–593. <https://doi.org/10.1029/95wr03528>
- Liu, Y., Wallace, C. D., Zhou, Y., Ershadnia, R., Behzadi, F., Dwivedi, D., et al. (2020). Influence of streambed heterogeneity on hyporheic flow and sorptive solute transport. *Water*, 12(6), 1547. <https://doi.org/10.3390/w12061547>
- Mackay, D. M., Freyberg, D. L., Roberts, P. V., & Cherry, J. A. (1986). A natural gradient experiment on solute transport in a sand aquifer: 1. Approach and overview of plume movement. *Water Resources Research*, 22(13), 2017–2029. <https://doi.org/10.1029/wr022013p02017>
- Neuman, S. P., Winter, C. L., & Newman, C. M. (1987). Stochastic theory of field-scale Fickian dispersion in anisotropic porous media. *Water Resources Research*, 23(3), 453–466. <https://doi.org/10.1029/wr023i003p00453>
- Pescimoro, E., Boano, F., Sawyer, A. H., & Soltanian, M. R. (2019). Modeling influence of sediment heterogeneity on nutrient cycling in streambeds. *Water Resources Research*, 55(5), 4082–4095. <https://doi.org/10.1029/2018wr024221>
- Proce, C. J., Ritzi, R. W., Dominic, D. F., & Dai, Z. (2004). Modeling multiscale heterogeneity and aquifer interconnectivity. *Groundwater*, 42(5), 658–670.
- Pryshlak, T. T., Sawyer, A. H., Stonedahl, S. H., & Soltanian, M. R. (2015). Multiscale hyporheic exchange through strongly heterogeneous sediments. *Water Resources Research*, 51(11), 9127–9140. <https://doi.org/10.1002/2015wr017293>
- Puyguiraud, A., Perez, L. J., Hidalgo, J. J., & Dentz, M. (2020). Effective dispersion coefficients for the upscaling of pore-scale mixing and reaction. *Advances in Water Resources*, 146, 103782. <https://doi.org/10.1016/j.advwatres.2020.103782>
- Rajaram, H., & Gelhar, L. W. (1993). Plume scale-dependent dispersion in heterogeneous aquifers: 1. Lagrangian analysis in a stratified aquifer. *Water Resources Research*, 29(9), 3249–3260. <https://doi.org/10.1111/j.1745-6584.2004.tb02720.x>
- Ramanathan, R., Ritzi, R. W., Jr., & Allen-King, R. M. (2010). Linking hierarchical stratal architecture to plume spreading in a Lagrangian-based transport model: 2. Evaluation using new data from the Borden site. *Water Resources Research*, 46(1). <https://doi.org/10.1029/2009wr007810>
- Ramanathan, R., Ritzi, R. W., Jr., & Huang, C. (2008). Linking hierarchical stratal architecture to plume spreading in a Lagrangian-based transport model. *Water Resources Research*, 44(4). <https://doi.org/10.1029/2007wr006282>
- Reeves, D. M., Benson, D. A., & Meerschaert, M. M. (2008a). Influence of fracture statistics on advective transport and implications for geologic repositories. *Water Resources Research*, 44(8). <https://doi.org/10.1029/2007wr006179>
- Reeves, D. M., Benson, D. A., & Meerschaert, M. M. (2008b). Transport of conservative solutes in simulated fracture networks: 1. Synthetic data generation. *Water Resources Research*, 44(5). <https://doi.org/10.1029/2007wr006069>
- Ritzi, R. W., Jr., Huang, L., Ramanathan, R., & Allen-King, R. M. (2013). Horizontal spatial correlation of hydraulic and reactive transport parameters as related to hierarchical sedimentary architecture at the Borden research site. *Water Resources Research*, 49(4), 1901–1913. <https://doi.org/10.1002/wrcr.20165>
- Ritzi, R. W., Jr., & Soltanian, M. R. (2015). What have we learned from deterministic geostatistics at highly resolved field sites, as relevant to mass transport processes in sedimentary aquifers? *Journal of Hydrology*, 531, 31–39. <https://doi.org/10.1016/j.jhydrol.2015.07.049>
- Rizzo, C. B., Nakano, A., & de Barros, F. P. (2019). Par2: Parallel random walk particle tracking method for solute transport in porous media. *Computer Physics Communications*, 239, 265–271. <https://doi.org/10.1016/j.cpc.2019.01.013>
- Rolle, M., Eberhardt, C., Chiogna, G., Cirpka, O. A., & Grathwohl, P. (2009). Enhancement of dilution and transverse reactive mixing in porous media: Experiments and model-based interpretation. *Journal of Contaminant Hydrology*, 110(3–4), 130–142. <https://doi.org/10.1016/j.jconhyd.2009.10.003>
- Rolle, M., Hochstetler, D., Chiogna, G., Kitanidis, P. K., & Grathwohl, P. (2012). Experimental investigation and pore-scale modeling interpretation of compound-specific transverse dispersion in porous media. *Transport in Porous Media*, 93(3), 347–362. <https://doi.org/10.1007/s11242-012-9953-8>
- Rubin, Y. (2003). *Applied stochastic hydrogeology*. Oxford University Press.
- Rubin, Y., Sun, A., Maxwell, R., & Bellin, A. (1999). The concept of block-effective macrodispersivity and a unified approach for grid-scale-and plume-scale-dependent transport. *Journal of Fluid Mechanics*, 395, 161–180. <https://doi.org/10.1017/s0022112099005868>
- Salamon, P., Fernandez-Garcia, D., & Gómez-Hernández, J. J. (2007). Modeling tracer transport at the MADE site: The importance of heterogeneity. *Water Resources Research*, 43(8). <https://doi.org/10.1029/2006wr005522>
- Sanchez-Vila, X., & Fernández-García, D. (2016). Debates—Stochastic subsurface hydrology from theory to practice: Why stochastic modeling has not yet permeated into practitioners? *Water Resources Research*, 52(12), 9246–9258. <https://doi.org/10.1002/2016WR019302>
- Sanchez-Vila, X., Guadagnini, A., & Carrera, J. (2006). Representative hydraulic conductivities in saturated groundwater flow. *Reviews of Geophysics*, 44(3). <https://doi.org/10.1029/2005RG000169>
- Soltanian, M. R., Behzadi, F., & de Barros, F. P. (2020). Dilution enhancement in hierarchical and multiscale heterogeneous sediments. *Journal of Hydrology*, 587, 125025. <https://doi.org/10.1016/j.jhydrol.2020.125025>
- Soltanian, M. R., & Ritzi, R. W. (2014). A new method for analysis of variance of the hydraulic and reactive attributes of aquifers as linked to hierarchical and multiscale sedimentary architecture. *Water Resources Research*, 50(12), 9766–9776. <https://doi.org/10.1002/2014wr015468>
- Soltanian, M. R., Ritzi, R. W., Dai, Z., & Huang, C. C. (2015a). Reactive solute transport in physically and chemically heterogeneous porous media with multimodal reactive mineral facies: The Lagrangian approach. *Chemosphere*, 122, 235–244. <https://doi.org/10.1016/j.chemosphere.2014.11.064>
- Soltanian, M. R., Ritzi, R. W., Huang, C. C., & Dai, Z. (2015b). Relating reactive solute transport to hierarchical and multiscale sedimentary architecture in a Lagrangian-based transport model: 2. Particle displacement variance. *Water Resources Research*, 51(3), 1601–1618. <https://doi.org/10.1002/2014wr016354>

- Srzić, V., Cvetkovic, V., Andricevic, R., & Gotovac, H. (2013). Impact of aquifer heterogeneity structure and local-scale dispersion on solute concentration uncertainty. *Water Resources Research*, 49(6), 3712–3728. <https://doi.org/10.1002/wrcr.20314>
- Stegen, J. C., Fredrickson, J. K., Wilkins, M. J., Konopka, A. E., Nelson, W. C., Arntzen, E. V., et al. (2016). Groundwater–surface water mixing shifts ecological assembly processes and stimulates organic carbon turnover. *Nature Communications*, 7(1), 1–12. <https://doi.org/10.1038/ncomms11237>
- Sudicky, E. A. (1986). A natural gradient experiment on solute transport in a sand aquifer: Spatial variability of hydraulic conductivity and its role in the dispersion process. *Water Resources Research*, 22(13), 2069–2082. <https://doi.org/10.1029/wr022i013p02069>
- Sudicky, E. A., & Illman, W. A. (2011). Lessons learned from a suite of CFB Borden experiments. *Groundwater*, 49(5), 630–648. <https://doi.org/10.1111/j.1745-6584.2011.00843.x>
- Thierrin, J., & Kitanidis, P. K. (1994). Solute dilution at the Borden and Cape Cod groundwater tracer tests. *Water Resources Research*, 30(11), 2883–2890. <https://doi.org/10.1029/94wr01983>
- Werth, C. J., Cirpka, O. A., & Grathwohl, P. (2006). Enhanced mixing and reaction through flow focusing in heterogeneous porous media. *Water Resources Research*, 42(12). <https://doi.org/10.1029/2005wr004511>
- Yong, Z., Benson, D. A., LaBolle, E. M., & Reeves, D. M. (2008). Fractional-RWHet: An enhanced solver for solute transport with both spatio-temporal memory and conditioning on local aquifer properties.
- Zavala-Sanchez, V., Dentz, M., & Sanchez-Vila, X. (2009). Characterization of mixing and spreading in a bounded stratified medium. *Advances in Water Resources*, 32(5), 635–648. <https://doi.org/10.1016/j.advwatres.2008.05.003>
- Zhang, Y., LaBolle, E., Reeves, D. M., & Russell, C. (2012). *Development of RWHet to simulate contaminant transport in fractured porous media* (No. 45244). Desert Research Institute, Nevada University.
- Zhang, Y., Labolle, E. M., Reeves, D. M., & Russell, C. (2013). Direct numerical simulation of matrix diffusion across fracture/matrix interface. *Water Science and Engineering*, 6(4), 365–379.
- Zheng, C., Bianchi, M., & Gorelick, S. M. (2011). Lessons learned from 25 years of research at the MADE site. *Groundwater*, 49(5), 649–662. <https://doi.org/10.1111/j.1745-6584.2010.00753.x>